

# Discovering Alarm Event Causality Based on Neural Point Process Modeling with Topology Constraint for Root Cause Analysis

Xiangxiang Zhang<sup>a,b,c</sup>, Wenkai Hu<sup>a,b,c,\*</sup> and R. Bhushan Gopaluni<sup>d</sup>

<sup>a</sup> School of Automation, China University of Geosciences, Wuhan 430074, China

<sup>b</sup> Hubei Key Laboratory of Advanced Control and Intelligent Automation for Complex Systems, Wuhan 430074, China

<sup>c</sup> Engineering Research Center of Intelligent Technology for Geo-Exploration, Ministry of Education, Wuhan 430074, China

<sup>d</sup> Department of Chemical and Biological Engineering, University of British Columbia, Vancouver, BC V6T 1Z3, Canada

## ARTICLE INFO

### Keywords:

Alarm & Event data  
causality discovery  
root cause analysis  
neural point process  
topology

## ABSTRACT

Fault propagation in industrial systems often leads to a surge in alarms, overwhelming operators and rendering the alarm system ineffective. Discovering causality between alarms is essential for operators to identify root cause alarms and address alarm floods, transforming overwhelming data into actionable diagnostic information. Existing methods for analyzing causal relations of alarms predominantly rely on process data, ignoring Alarm & Event (A&E) data that is directly related to faults. Further, purely data-driven approaches ignore the topology between systems, leading to spurious causal relations. Therefore, this research proposes a new Alarm Causality discovery method based on Neural Point Process modeling (AlarmCNP). The contributions are threefold: 1) A neural point process modeling method for A&E data is proposed based on alarm encoding and Continuous-Time Long Short Term Memory (CTLSTM) to calculate the conditional intensity; 2) a new causality measurement is designed based on the conditional causal intensity to identify Granger causality and measure the causal strength; 3) a system topology constrained causality inference method is presented to eliminate spurious causal relations and determine the final causal relations. The effectiveness of the proposed method is validated through case studies involving two public industrial models, namely, the two-tank system model and the Vinyl Acetate Monomer model.

## 1. Introduction

In a contemporary industrial facility, there exists an abundance of interconnected devices and control loops. When a fault occurs, it is prone to propagate throughout the flow of information and material, consequently instigating a multitude of alarms (Wang, Hu and Chen, 2024). This has the potential to hinder the operator's ability to address the situation proficiently, thereby rendering the alarm system ineffective and exacerbating the circumstances. By means of alarm cause-effect analysis, one can identify the root causes of numerous alarms, enabling operators to prioritize their attention towards these root alarms and effectively handle them (Alinezhad, Roohi and Chen, 2022; Song, Zhao, Huang and Wu, 2022).

The current body of literature encompasses two principal categories of methodologies to address this issue, specifically, knowledge-based approaches and data-driven techniques. In knowledge-based methods, alarm causality discovery relies primarily on qualitative process information, such as Piping and Instrumentation Diagrams (P&IDs), and the expert knowledge (Landman and Jämsä-Jounela, 2019). Commonly used methods in this category include signed directed graphs (Yang, Xiao and Shah, 2013), adjacency matrices (Jiang, Patwardhan and Shah, 2009), and multilevel flow models (Nielsen, Gofuku, Zhang, Ravn and Lind, 2020). These methods aim to uncover fault propagation paths among different process units, enabling the

localization of the root cause in specific abnormal situations and subsequently identifying the most plausible root cause. However, obtaining the necessary process knowledge from industrial processes is often a time-consuming and challenging endeavor (Alinezhad et al., 2022).

To overcome this limitation and reduce reliance on human effort, data-driven cause-effect analysis has been developed. Most existing data-driven methods are based on the time series of process variables. Classical methods include the Granger causality, Transfer Entropy (TE), and Bayesian Networks (BNs) (Alinezhad et al., 2022). For instance, a multi-level predictive relation aggregation method based on Granger causality is developed in Zhao, Song and Zhao (2025) to discover causality in nonlinear processes. In Tank, Covert, Foti, Shojaie and Fox (2022), Granger causality based on recurrent neural network architecture was introduced to mitigate the challenges of non-stationary data. Moreover, Multiscale Partial Symbolic TE (MPSTE) (Duan, Zhao and Wu, 2023) and Information Granulation-based TE (IGTE) (Zhang, Hu, Yang, Cao and Wu, 2023) were proposed for causality inference in nonlinear processes. By converting the original time series into symbols or granules and then estimating the probability density function, these methods are well-suited for handling non-stationary data. In addition, as a probabilistic graphical model, BNs and improved methods based on BNs were employed to capture causality by constructing directed acyclic graphs (Kumari, Bhadriraju, Wang and Kwon, 2022; Luo, Gopaluni, Cao, Wang and Cheng, 2023; Yang, Lan, Qiu and Zhang, 2025).

Alarm data, as a supplement of the process data, has also been exploited for causality discovery (Alinezhad et al.,

\*Corresponding author

✉ xiangxiangzhang@cug.edu.cn (X. Zhang); wenkaihu@cug.edu.cn (W. Hu); bhushan.gopaluni@ubc.ca (R.B. Gopaluni)

2022). For instance, Yu and Yang (2015) pioneered the use of binary alarm series directly for cause-effect analysis, enabling the discovery of causal relations in abnormal situations and facilitating alarm management. Similarly, utilizing binary alarm series, a Normalized TE (NTE) (Hu, Wang, Chen and Shah, 2017) and a K2 algorithm for structural learning of BNs (de Abreu, Nunes, Guedes and Silva, 2021) were proposed to discover causal relations between industrial alarm variables. Further, an alarm causality discovery approach based on multi-valued alarm series (including -1, 0, and 1) was proposed to establish an alarm propagation network during an alarm flood (Luo, Gopaluni, Xu, Cao and Zhu, 2020). The alarm data discussed, whether binary or multi-valued alarm series, is numerical data. The methods applied to such data the same as those for process signals.

There is another class of causality discovery methods that utilize a different form of alarm data, namely, the Alarm & Event (A&E) data, which data consists of textual event messages that can be directly available in the alarm historian. Some causality discovery methods based on Hawkes process (Xu, Farajtabar and Zha, 2016) and topological Hawkes process (Cai, Wu, Qiao, Hao, Zhang and Zhang, 2024) were applied to infer causality based on such event data and demonstrated to be effective. These methods directly model the textual event sequences while assuming that historical events always exert a positive excitation on future events. However, real industrial processes often struggle to meet the stringent assumptions required by the Hawkes process, making these methods challenging to apply for modeling A&E data.

According to the above literature survey, there exist three major challenges with the existing methods: First, existing methods are mainly based on the numerical time series and have high computational complexity, whereas the A&E data as a condensed simpler form of alarm signals is usually overlooked. Then, even though Xu et al. (2016) and Cai et al. (2024) provide a new approach for causality discovery using A&E data, their assumption is too stringent for actual industrial processes, compromising the performance in real applications. Last, existing methods are often purely data-driven, ignoring the topological connections between systems, which may lead to spurious causal relations.

Motivated by the above practical issues, this research proposes a new Alarm Causality discovery method based on Neural Point Process modeling (AlarmCNPP). The contributions are threefold as follows:

- 1) A neural point process modeling method for A&E data is proposed based on alarm encoding and Continuous-Time Long Short Term Memory (CTLSTM) to calculate the conditional intensity.
- 2) A new causality measurement is designed based on the conditional causal intensity to identify Granger causality and measure the causal strength.
- 3) A system topology constrained causality inference method is presented to eliminate spurious causal relations and determine the final causal relations.

The effectiveness of the proposed method is validated through two industrial case studies.

The rest of this paper is organized as follows: Section 2 presents the problem. Section 3 proposes the alarm causality discovery approach. Section 4 provides two case studies to show the effectiveness, and Section 5 gives the conclusions.

## 2. Problem description

In complex industrial systems, when abnormalities occur, a cascade of alarm events may ensue and propagate rapidly. Discovering the causal relations between these alarms and locating their root causes is essential for making informed decisions and implementing corrective actions in response to alarms. Let  $\mathbb{D} = \{(a_j, t_j) \mid a_j \in \mathcal{A}, j \in \mathbb{N}^+\}$  represent an A&E log gathered over a specific historical duration, where  $a_j$  signifies the  $j$ th alarm in  $\mathbb{D}$ ,  $t_j$  represents the timestamp of  $a_j$ ,  $\mathcal{A}$  denotes the set of alarm tags in the alarm system, and  $\mathbb{N}^+$  indicates natural numbers. An alarm event sequence comprises alarm events arranged in chronological order, i.e.,

$$S = \langle e_1, e_2, \dots, e_{|S|} \rangle, \quad (1)$$

where  $\langle \cdot \rangle$  represents a sequence,  $|S|$  indicates the length of  $S$ , and  $e_i$  denotes the  $i$ th alarm event. An alarm event  $e_i$  records the alarm tag and its time stamp, such that

$$e_i = (a_i, t_i), \quad (2)$$

where  $a_i \in \mathcal{A}$ , and  $t_i$  denotes the time stamp of  $a_i$ .

Given an alarm event sequence  $S$ , the purpose is to discover the causal relations between alarms, so as to identify the root cause. A typical approach involves constructing a Temporal Point Process (TPP) model for event sequence (Xu et al., 2016). Unlike traditional time series models that assume fixed time intervals, TPP can be used to model asynchronous events occurring at irregular times, making TPP particularly suitable for modeling alarm sequences, where the triggered alarm events usually appear with irregular time intervals other than at predetermined time stamps. TPP employs an explicitly defined Conditional Intensity Function (CIF) to quantify event occurrence rates and capture temporal dependencies between events, naturally modeling how past alarms influence the likelihood of future ones (Xiao, Yan, Farajtabar, Song, Yang and Zha, 2019).

Within the realm of TPP, the self-exciting point process, known as the Hawkes process, is frequently utilized to unveil causal relations among events (Xu et al., 2016; Cai et al., 2024). The Hawkes process models causality by assuming that past events can increase the likelihood of future events through explicit excitation. It reflects that events are interconnected, with one event potentially impacting others. This causal modeling relies on the CIF, which quantifies how each past event influences the current event's probability with a time-decaying effect. The CIF characterizing the Hawkes process for alarm events of tag  $a_j$  is outlined as follows:

$$\lambda_{a_j}(t) = \mu_{a_j} + \sum_{t_m < t} \phi_{a_j, a_i}(t - t_m) \quad (3)$$

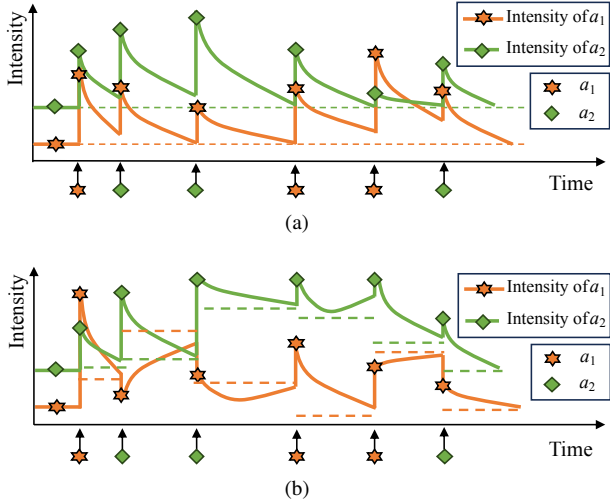


**Fig. 1:** Schematic diagram of conditional intensity functions. (a) Hawkes process. The intensity function is represented as a solid line, and the dashed line represents the base rate. In a Hawkes process, each alarm excites the occurrence of its own and other alarms. (b) Neural point process. The intensity functions are represented as continuous parametric curves (solid lines), with dashed lines indicating the steady-state asymptotes.

where  $\mu_{a_j}$  is the base rate for alarms of tag  $a_j$ , which refers to the intensity inherent in  $a_j$ , regardless of historical alarms;  $\phi_{a_j, a_i}(t - t_m)$  represents the impact of historical alarm of tag  $a_i$  on current alarm of tag  $a_j$ ,  $t_m$  denotes the time when the last alarm occurs. In addition, a schematic diagram describing the change of its CIF over time is shown in Fig. 1(a). It contains two alarms  $a_1$  and  $a_2$ , which occur multiple times respectively. When an alarm occurs, the corresponding intensities of  $a_1$  and  $a_2$  are elevated to various degrees, but then will decay toward their base rates  $\mu_{a_1}$  and  $\mu_{a_2}$ .

However, the assumption of Hawkes process is overly stringent to capture the complexities of real industrial processes, because alarm causality can be both excitatory and inhibitory. For example, in a water tank system with heat exchange, when the input cold water temperature  $T_0$  drops suddenly, a low limit alarm of  $T_0$  may appear and in turn excite the tank temperature  $T_1$  to decrease, triggering a low limit alarm of  $T_1$ . Accordingly, the temperature controller would quickly increase the steam flow rate  $F$  in the heat exchange system to raise the tank temperature  $T_1$ . As a result, there would be a high limit alarm due to the increased flow rate  $F$ , which then inhibits the low limit alarm of  $T_1$ .

In order to explore such relationships between alarms, a more general, flexible, and learnable NPP modeling method is needed. Fig. 1(b) illustrates the schematic diagram of the CIF utilized in the NPP. Unlike Hawkes process, it is not restricted to a specific assumption and is more versatile. In this example, the low limit alarm of  $T_1$ , namely  $a_1$ , excites both itself and the high limit alarm of  $F$ , namely  $a_2$ , while  $a_2$  excites itself but inhibits  $a_1$ . These immediate effects are illustrated by the sudden jumps in intensity. Additionally, the alarms have longer-term effects, as shown by the shifts in the

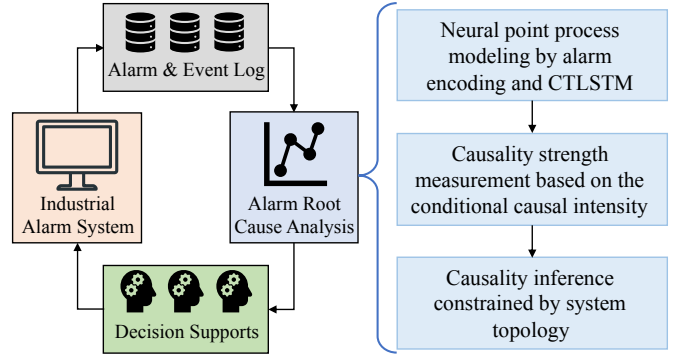


**Fig. 2:** The framework of the proposed method.

asymptotic dashed lines. The NPP can learn and model the CIF directly from historical event sequences, without relying on a predetermined parametric model.

In view of the above discussion, this paper proposes a new alarm causality discovery method based on the NPP modeling. The performance of the proposed method is further enhanced by integrating the system topology in causality inference. The framework of the proposed method is illustrated in Fig. 2 and summarized as follows:

- The historical alarm event sequence is modeled by alarm encoding and CTLSTM; the CIF is learned and simulated to capture the impacts between alarms.
- By considering the historical information of alarm events, a new measurement based on the Conditional Causal Intensity (CCI) is devised to measure the Granger causality strength between alarms.
- The system topology is exploited as a constraint for causality inference to eliminate spurious causal relations that lack physical connections.

Through alarm cause-effect analysis, operators can identify the underlying causes of various alarms, providing them with valuable decision support. This empowers operators to prioritize their attention on the critical alarms and address these issues more effectively.

### 3. The Proposed Method

This section presents the proposed alarm causality discovery method named AlarmCNPP. It offers the NPP modeling by alarm encoding and CTLSTM, causality strength measurement based on the CCI, and causality inference constrained by system topology.

#### 3.1. NPP modeling by alarm encoding and CTLSTM

A more flexible NPP modeling method based on alarm encoding and CTLSTM is proposed for A&E data. It captures various relationships between alarms, including excitation and inhibition, by simulating and learning the CIF.

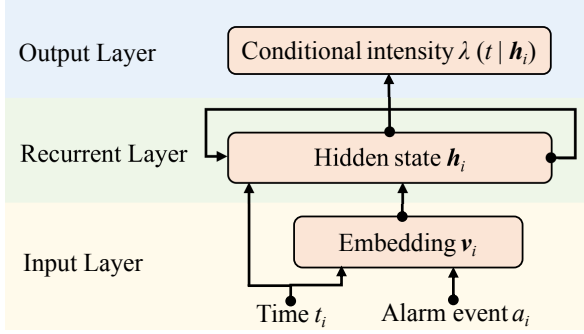


**Fig. 3:** The alarm event sequence modeling architecture based on the proposed NPP modeling method.

Alarm encoding can embed textual alarms into numerical vectors (Hu, Yang, Li, Cao and Wu, 2024; Zhang, Hu, Al-Dabbagh and Wang, 2024). Compared with traditional LSTM, CTLSTM can model event sequence with irregular time intervals, making it more suitable to the A&E data in this study. The alarm event sequence modeling architecture is presented in Fig. 3. The model takes an alarm event sequence as input and outputs the condition intensities of alarms. The specific process is as follows:

Given an alarm event sequence  $S = \langle e_1, e_2, \dots, e_{|S|} \rangle$ , its CIF is given by

$$\lambda(t) = \sum_{a_j \in \mathcal{A}} \lambda_{a_j}(t), \quad (4)$$

where  $\lambda_{a_j}(t)$  is the CIF for the alarm events of tag  $a_j$ , i.e.,

$$\lambda_{a_j}(t) = f_{a_j}(\mathbf{w}_{a_j}^\top \mathbf{h}(t)), \quad (5)$$

where  $f()$  is the scaled “softplus” function  $f(x) = \text{slog}(1 + \exp(x/s))$ ;  $s$  is a separate scale parameter to learn for each alarm tag, and it adapts to the rate of that alarm tag. The weight matrix  $\mathbf{w}_{a_j}$  is learned during the training process; the hidden state  $\mathbf{h}(t)$  is derived by inputting the historical alarm event sequence into the CTLSTM.

However, since the alarm event sequence consists of textual data, it cannot be used directly for calculations to obtain the hidden state  $\mathbf{h}(t)$ . Therefore, alarm encoding based on feature embedding (Xiao et al., 2019) is used to encode textual information into vectors. For the sequence  $S$ , each alarm event  $e_i = (a_i, t_i)$  is encoded into a vector that summarizes both the temporal and the alarm tag information. The encoding vector of  $e_i$  is

$$\mathbf{v}_i = [\psi(t_i); W_a^\top \mathbf{a}_i], \quad (6)$$

where  $\psi()$  is a pre-specified function that transforms the elapsed time into one or more temporal features, it can be simply chosen as an identity function,  $W_a$  is the embedding matrix for alarms, and  $\mathbf{a}_i$  is the one-hot encoding of  $a_i$ . The embedding matrix  $W$  is multiplied by each alarm’s one-hot encoded vector to produce an embedded vector representing

the alarm, which is then used for computation and inference. Although the dimensionality of the one-hot vectors increases with the number of alarms, the dimension of the embedding vectors remains fixed; thus, one-hot encoding increases the model parameters, but has little influence to the computation time.

The following equations give the update for a layer of memory cells  $\mathbf{h}(t_{m+1})$ , where  $\mathbf{h}(t_m)$  stands for the previous output at the previous sequence step in the same layer (Mei and Eisner, 2017). The memory unit candidate  $\mathbf{z}_{m+1}$ , input gate  $\mathbf{g}_{m+1}$ , forgetting gate  $\mathbf{f}_{m+1}$ , and output gate  $\mathbf{o}_{m+1}$  for the  $(m+1)$ th event  $e_{m+1}$  are calculated as

$$\begin{cases} \mathbf{g}_{m+1} = \sigma(\mathbf{W}_{xg}\mathbf{v}_m + \mathbf{W}_{hg}\mathbf{h}(t_m) + \mathbf{b}_g), \\ \mathbf{f}_{m+1} = \sigma(\mathbf{W}_{xf}\mathbf{v}_m + \mathbf{W}_{hf}\mathbf{h}(t_m) + \mathbf{b}_f), \\ \mathbf{o}_{m+1} = \sigma(\mathbf{W}_{xo}\mathbf{v}_m + \mathbf{W}_{ho}\mathbf{h}(t_m) + \mathbf{b}_o), \\ \mathbf{z}_{m+1} = \tanh(\mathbf{W}_{xz}\mathbf{v}_m + \mathbf{W}_{hz}\mathbf{h}(t_m) + \mathbf{b}_z), \end{cases} \quad (7)$$

where  $\mathbf{v}_m$  is the  $m$ th elements in the embedded alarm event sequence;  $\mathbf{W}_{ij}$  (with  $i = x, h$  and  $j = z, g, f, o$ ) denotes the weight matrices corresponding to different inputs ( $\mathbf{v}_m$  or  $\mathbf{h}(t_m)$ ) and representing different gate mechanisms;  $\mathbf{b}_j$  indicates the corresponding bias vector;  $\sigma()$  stands for the sigmoid function;  $\tanh()$  represents the tanh function.

For  $t \in (t_{m-1}, t_m]$ ,  $\mathbf{c}(t)$  is a continuous function changing over time from the CTLSTM memory cell initial state  $\mathbf{c}_m$  to the cell state decaying target  $\bar{\mathbf{c}}_m$  (Mei and Eisner, 2017). For  $\bar{\mathbf{c}}_m$ , it also has an input gate  $\bar{\mathbf{g}}$  and a forget gate  $\bar{\mathbf{f}}$ , which are given by

$$\begin{cases} \bar{\mathbf{g}}_{m+1} = \sigma(\bar{\mathbf{W}}_{xg}\mathbf{v}_m + \bar{\mathbf{W}}_{hg}\mathbf{h}(t_m) + \bar{\mathbf{b}}_g), \\ \bar{\mathbf{f}}_{m+1} = \sigma(\bar{\mathbf{W}}_{xf}\mathbf{v}_m + \bar{\mathbf{W}}_{hf}\mathbf{h}(t_m) + \bar{\mathbf{b}}_f). \end{cases} \quad (8)$$

Then,  $\mathbf{c}_{m+1}$  and  $\bar{\mathbf{c}}_{m+1}$  are given by

$$\begin{cases} \mathbf{c}_{m+1} = \mathbf{f}_{m+1} \odot \mathbf{c}(t_m) + \mathbf{g}_{m+1} \odot \mathbf{z}_{m+1}, \\ \bar{\mathbf{c}}_{m+1} = \bar{\mathbf{f}}_{m+1} \odot \bar{\mathbf{c}}_m + \bar{\mathbf{g}}_{m+1} \odot \mathbf{z}_{m+1}, \end{cases} \quad (9)$$

where  $\odot$  is the Hadamard (element-wise) product. During  $(t_m, t_{m+1}]$ , the cell state  $\mathbf{c}(t)$  at time  $t$  can be derived based on Eq. (9), i.e.,

$$\mathbf{c}(t) = \bar{\mathbf{c}}_{m+1} + (\mathbf{c}_{m+1} - \bar{\mathbf{c}}_{m+1}) \exp(-\delta_{m+1}(t - t_m)), \quad (10)$$

where  $\delta$  is the parameter to control decaying pace. It is given by

$$\delta_{m+1} = f(\mathbf{W}_{x\delta}\mathbf{v}_m + \mathbf{W}_{h\delta}\mathbf{h}(t_m) + \mathbf{b}_\delta). \quad (11)$$

Then, the hidden state  $\mathbf{h}(t)$  at time  $t$  is obtained as

$$\mathbf{h}(t) = \mathbf{o}_m \odot \tanh(\mathbf{c}(t)). \quad (12)$$

Next, according to the hidden state  $\mathbf{h}(t)$ , the CIF  $\lambda(t)$  can be calculated. The weight matrices in the above equations are learned during the training process to optimize the CTLSTM model for capturing temporal dependencies.

To train the NPP model, the commonly employed maximum likelihood estimation method is used here. Model parameters are learned by maximizing the log-likelihood. For an alarm event sequence  $S = \langle e_1, e_2, \dots, e_{|S|} \rangle$  over an observation interval  $[0, T]$ , given its CIF  $\lambda(t)$ , the log-likelihood is defined as the sum of the log-intensities of the events that happened, minus an integral of the total intensities over the observation interval  $[0, T]$ :

$$L = \sum_{i=1}^{|S|} \log \lambda(t_i) - \int_{t=0}^T \lambda(t) dt, \quad (13)$$

where  $\sum_{i=1}^{|S|} \log \lambda(t_i)$  is the sum of the log-intensity functions of past events, and  $\int_{t=0}^T \lambda(t) dt$  corresponds to the log-likelihood of infinitely many non-events. The integral term can be obtained through Monte Carlo approximation (Mei and Eisner, 2017).

**Remark 1:** Compared to the Hawkes process, the NPP relaxes strict assumptions by using alarm encoding and CTLSTM to learn complex, non-parametric CIF directly from historical data. While Hawkes processes assume fixed exponential decay and linear influence of past events, NPP can learn complex temporal dependencies without predefined kernels or decay rates (Lin, Tan, Wu, Liu, Gao and Li, 2025). This allows NPP to rely only on historical event sequences to model both excitatory and inhibitory relationships more flexibly.

### 3.2. Causality strength measurement based on the CCI

A new causality strength measurement is devised based on the proposed NPP model to identify causal relations among alarms. This measurement is inspired by the concept of Granger causality, which posits that if including the historical data of variable  $X$  improves the prediction of variable  $Y$  beyond using only  $Y$ 's past, then  $X$  can be regarded as a cause of  $Y$  (Kathari and Tangirala, 2022). Extending this idea, causal links between two alarms,  $a_i$  and  $a_j$ , are detected by comparing predictions of the conditional intensity under different historical information involving these alarms. Specifically, the designed causality measurement comprises two steps:

#### 3.2.1. Calculation of the CCI to discover Granger causality between alarms

To discover Granger causality between alarms, a novel causality measurement CCI is proposed based on the conditional intensity. When calculating the conditional intensity of alarm events of tag  $a_i$ , if only the historical information of  $a_i$  is considered, the CIF is defined as  $\lambda_{a_i}(t|\mathbf{h}_{a_i})$ . If the historical information of  $a_i$  and  $a_j$  are considered simultaneously, the CIF of alarm events of tag  $a_i$  is defined as  $\lambda_{a_i}(t|\mathbf{h}_{a_i,a_j})$ . They can be calculated by

$$\lambda_{a_i}(t|\mathbf{h}_{a_i}) = f_{a_i}(\mathbf{w}_{a_i}^\top \mathbf{h}_{a_i}(t)), \quad (14)$$

$$\lambda_{a_i}(t|\mathbf{h}_{a_i,a_j}) = f_{a_i}(\mathbf{w}_{a_i}^\top \mathbf{h}_{a_i,a_j}(t)). \quad (15)$$

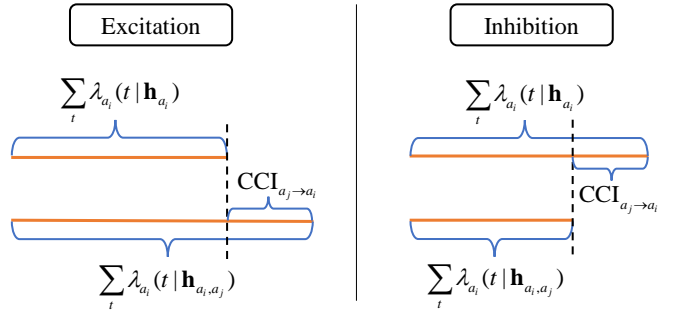


**Fig. 4:** Schematic diagram of CCI, including excitation and inhibition.

In this research, the concept of causality rooted in prediction is applied to predict conditional intensity. By considering the historical information of different alarm events, the predictive effects of conditional intensity are assessed, leading to an analysis of causal relations between various alarms based on changes in predictive effects. Building upon this concept, a novel causality measurement CCI is formulated, with a detailed explanation provided in Definition 1.

**Definition 1 (Conditional Causal Intensity).** *If the historical occurrence of alarm  $a_j$  impacts (such as excitation or inhibition) to the future conditional intensity  $\lambda_{a_i}(t|\mathbf{h}_{a_i,a_j})$  of alarm  $a_i$ , alarm  $a_j$  is considered a Granger cause for alarm  $a_i$ . Otherwise, alarm  $a_j$  is deemed to be a Granger non-cause for alarm  $a_i$ . The schematic diagram of CCI is shown in Fig. 4, illustrating both excitation and inhibition cases.*

Based on Definition 1, the Granger causality between alarms can be determined by calculating the conditional intensity under various historical conditions of alarms. The value of CCI from alarm  $a_j$  to  $a_i$  is defined as follows:

$$CCI_{a_j \rightarrow a_i} = \sum_t \lambda_{a_i}(t|\mathbf{h}_{a_i,a_j}) - \sum_t \lambda_{a_i}(t|\mathbf{h}_{a_i}). \quad (16)$$

The causality measurement CCI is designed for A&E data based on the definition of Granger causality. It is calculated from the conditional intensity of the alarm events, providing a new tool for discovering causal relations between alarms.

#### 3.2.2. Normalization of the CCI to determine the causal strength

Further, due to the significant variations in conditional intensity among different alarm events and the inconsistent number of occurrences, the resulting CCI values may exhibit a large gap, rendering direct comparison challenging. Consequently, it is necessary to normalize the calculated CCI for comparative analysis of the causal relations between alarms. As the values of CCI are dependent on  $\lambda_{a_i}(t|\mathbf{h}_{a_i,a_j})$  and  $\lambda_{a_i}(t|\mathbf{h}_{a_i})$ , a normalized metric, termed Normalized CCI (NCCI), is proposed and defined as:

$$NCCI_{a_j \rightarrow a_i} = \frac{CCI_{a_j \rightarrow a_i}}{\sum_t \lambda_{a_i}(t|\mathbf{h}_{a_i,a_j}) + \sum_t \lambda_{a_i}(t|\mathbf{h}_{a_i})}, \quad (17)$$

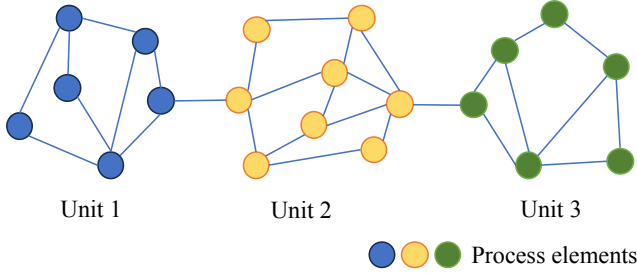


**Fig. 5:** An example of a process topology.

where  $\text{NCCI}_{a_j \rightarrow a_i}$  denotes the value of NCCI from  $a_j$  to  $a_i$ . The range of  $\text{NCCI}_{a_j \rightarrow a_i}$  is  $(-1, 1)$ . Specifically, when  $\text{CCI}_{a_j \rightarrow a_i} < 0$ , the range of  $\text{NCCI}_{a_j \rightarrow a_i}$  is  $(-1, 0)$ ; when  $\text{CCI}_{a_j \rightarrow a_i} \geq 0$ , the range of  $\text{NCCI}_{a_j \rightarrow a_i}$  is  $[0, 1]$ .

**Remark 2:** Compared to traditional Granger causality, CCI differs in the following aspects: 1) CCI measures the strength of excitation or inhibition based on the conditional intensity of alarm events, while traditional Granger causality examines the causal relations by comparing the restricted and unrestricted residual sums of squares in linear vector-autoregression; 2) CCI is suitable for event sequences and can capture nonlinear relationships, whereas traditional Granger causality applies only to continuous-valued data and detects linear relations; 3) the normalized version NCCI allows for quantitative measurement of causality strength.

### 3.3. Causality inference constrained by system topology

The causal relations can be identified based on Section 3.2. However, this purely data-driven approach ignores the real physical connections, resulting in spurious causal relations. To mitigate this issue, the system topology is incorporated into the alarm causality inference. Fig. 5 illustrates the visual example of a system topology. In actual industrial systems, there are usually several units corresponding to different processes, with each unit composed of multiple process elements.

Given the set of process elements  $P = \{p_1, p_2, \dots, p_{|P|}\}$ , the process topology can be represented as  $G_P$ , where  $p_g$  denotes the  $g$ th element and  $|P|$  signifies the total number of elements. If  $E_P$  represents the undirected edge set, then the process topology  $G_P = (P, E_P)$  can be expressed by the process topological adjacency matrix  $\mathbf{T}$ , with each entry  $T_{gh}$  defined as

$$T_{gh} = \begin{cases} 1, & \text{if } (p_g, p_h) \in E_P, \\ 0, & \text{otherwise,} \end{cases} \quad (18)$$

where  $p_g$  and  $p_h$  represent two individual edge connecting elements; when  $T_{gh} = 1$ , it indicates a topological connection exists between the two elements  $p_g$  and  $p_h$ . The process topology matrix  $\mathbf{T}$  is a symmetric matrix consisting of 0 and 1, i.e.,  $T_{gh} = T_{hg}$ .

Initially, process flow diagrams and P&IDs can be utilized to identify the process units and various distinct process elements (nodes) connected to each unit. Subsequently, leveraging prior knowledge such as material flow, energy transfer, and control logic, the connection relationships between process units are established, followed by the connections among specific process elements (Yang, Duan, Shah and Chen, 2014; Rahaman, Alinezhad and Chen, 2024). Several common approaches have been proposed to capture topology from process knowledge, including signed directed graph model, rule-based modeling, and the extraction of process topology from web languages. Details of these methods can be referred to Yang et al. (2014).

By following the procedure outlined above, the process elements and units associated with the analyzed alarms are identified. The established system topology serves as a crucial constraint that effectively narrows the search space for learning causal relations. This ensures that the analysis concentrates exclusively on causal connections with practical significance. As a result, the inferred causal links become sparse, filtering out spurious connections and accurately reflecting the true underlying dependencies within the system.

Specifically, when calculating  $\lambda_{a_i}(t|\mathbf{h}_{a_i, a_j})$ , the topological connection between the process elements  $p_g$  and  $p_h$  associated with alarms  $a_i$  and  $a_j$  serves as a constraint. The influence of  $a_j$  on  $a_i$  is only meaningful if there is a topological connection between  $p_g$  and  $p_h$ , specifically when  $T_{gh} = 1$ . Therefore, by considering the process topology, Eq. (15) is revised as

$$\lambda_{a_i}(t|\mathbf{h}_{a_i, a_j}) = \begin{cases} f_{a_i}(\mathbf{w}_i^\top \mathbf{h}_{a_i, a_j}), & \text{if } T_{gh} = 1, \\ \lambda_{a_i}(t|\mathbf{h}_{a_i}), & \text{otherwise.} \end{cases} \quad (19)$$

In addition, due to the influence of factors such as noise, the NCCI between two unrelated alarms is not strictly zero but rather takes on a certain value. Therefore, a threshold calculation method for determining the causal relationship of alarms is designed using the Monte Carlo approach based on the surrogate sequences (Zhang et al., 2023; Hu et al., 2017). Given the alarm event sequence  $S$ , multiple surrogate sequences are randomly generated to calculate the NCIs. The surrogate sequence  $S^{\text{th}}$  should have the same length and the same probability of alarm occurrences as  $S$ . Specifically,  $S^{\text{th}}$  is generated with multinomial distribution satisfying the following conditions:

- The sequence length of  $S^{\text{th}}$  is the same as that of  $S$ .
- The number of unique alarm tags in  $S^{\text{th}}$  is the same as in  $S$ . Since the probability of each alarm tag occurring is predetermined, they are independent of one another.
- The probability of each alarm tag occurring in  $S^{\text{th}}$  is equal to the proportion of each alarm tag in  $S$ .

The threshold  $\text{NCCI}^{\text{th}}$  is determined by calculating the mean of the NCIs obtained from multiple surrogate sequences and adding or subtracting six times the standard deviation. When  $\text{NCCI}_{a_j \rightarrow a_i} > 0$ , if  $\text{NCCI}_{a_j \rightarrow a_i} \geq \text{NCCI}_{a_j \rightarrow a_i}^{\text{th}}$ ,

it indicates an exciting causal relationship from  $a_j$  to  $a_i$ ; otherwise, no causal relation exists from  $a_j$  to  $a_i$ . Conversely, when  $\text{NCCI}_{a_j \rightarrow a_i} < 0$ , if  $\text{NCCI}_{a_j \rightarrow a_i} \leq \text{NCCI}_{a_j \rightarrow a_i}^{\text{th}}$ , it indicates an inhibitory causal relationship from  $a_j$  to  $a_i$ ; otherwise, no causal relation exists from  $a_j$  to  $a_i$ .

After the previous steps, a binary causal matrix  $\mathbf{C} \in \{0, 1\}^{n \times n}$  is obtained to represent the causal relations among alarm variables, where  $C_{ij} = 1$  indicates a direct causal relationship from alarm  $a_i$  to  $a_j$ . To identify the root cause variables clearly, a root cause ranking score  $R(a_i)$  for each alarm  $a_i$  is designed as

$$R(a_i) = \frac{R_1(a_i) + R_2(a_i) + R_3(a_i)}{3}, \quad (20)$$

where  $R_1(a_i)$  denotes the topological originality score that measures the upstream node's influences on an alarm;  $R_2(a_i)$  represents the influence propagation score that measures the downstream impact scope, reflecting the potential consequence magnitude of an alarm;  $R_3(a_i)$  indicates the structural importance score that combines in-degree and out-degree to evaluate a node's outgoing influence to its incoming influence, reflecting its structural role in the causal network. These three scores are given by

$$\begin{cases} R_1(a_i) = \frac{1}{D_{\text{in}}(a_i)+1}, \\ R_2(a_i) = \frac{\Omega(a_i)}{\max_j \Omega(a_j)}, \\ R_3(a_i) = \frac{D_{\text{out}}(a_i)/(D_{\text{in}}(a_i)+1)}{\max_j (D_{\text{out}}(a_j)/(D_{\text{in}}(a_j)+1))}, \end{cases} \quad (21)$$

where  $D_{\text{in}}(a_i) = \sum_{j=1}^n C_{ji}$  is the in-degree of  $a_i$ , representing the number of direct causal predecessors;  $D_{\text{out}}(a_i) = \sum_{j=1}^n C_{ij}$  indicates the out-degree of  $a_i$ , counting its direct causal successors;  $\Omega(a_i) = \sum_{j=1}^n \Omega_{ij} - 1$  denotes the number of nodes reachable from  $a_i$ , quantifying the propagation scope of potential cascading effects, where  $\Omega_{ij} = 1$  if there exists a directed path from  $a_i$  to  $a_j$ , and 0 otherwise. Thereby, the resulting root cause ranking score  $R(a_i)$  enables effective identification of true root causes from the perspectives of the topological originality, influence propagation, and structural importance.

**Remark 3:** The computational complexity of the proposed AlarmCNPP is expressed as  $O(|S|(E+n^2)h^2)$ , which consists of two parts: 1)  $O(|S|Eh^2)$  for NPP modeling with CTLSTM, where  $|S|$  denotes total number of observed alarm events,  $E$  is the training epochs, and  $h$  represents the hidden dimension; 2)  $O(|S|n^2h^2)$  for causality inference, where  $n$  denotes the number of unique alarms. For comparison, the computational complexities of the Hawkes Process (HP) and Topological Hawkes Process (THP) are  $O(|S|^3n^2IM)$  and  $O(|S|^3n^2K)$ , respectively, where  $I$  is the number of expectation maximization iterations,  $M$  denotes the number of basis functions, and  $K$  indicates the maximum topological distance; the computational complexity of TE is  $O(n^2(L+2^{(k+l+1)}))$ , where  $k$  and  $l$  are the orders of variables,  $L = T/\Delta t$  denotes the length of binary sequences,  $T$  is the observation time, and  $\Delta t$  indicates the discretization time

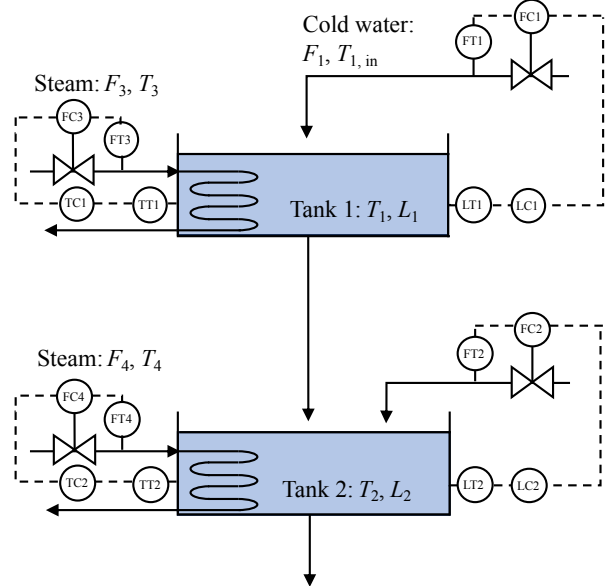


Fig. 6: Process diagram of two-tank system (Lindner et al., 2019).

interval and typically  $L \gg |S|$ . Accordingly, the following conclusions are drawn: 1) The computational complexity of AlarmCNPP scales linearly with  $|S|$ , whereas both HP and THP scale cubically, making AlarmCNPP more efficient than HP and THP as  $|S|$  has a major impact on the computation; 2) AlarmCNPP is also more efficient than TE given  $L$  much greater than  $|S|$ , as TE needs to convert the  $|S|$  alarm events into dense binary alarm series of length  $L$ . In addition, the quadratic term  $n^2$  is common to all causality discovery methods, as all possible alarm pairs must be evaluated. In the proposed AlarmCNPP, through topology constraints, the actual number of pairs can be reduced, further improving computational efficiency.

## 4. Case studies

This section provides two case studies to demonstrate the effectiveness of the proposed method, including a two-tank system and the Vinyl Acetate Monomer (VAM) model.

### 4.1. Case 1: Two-tank system

The primary model of the two-tank system was constructed in Simulink (Lindner, Auret, Bauer and Groenewald, 2019). This model has been utilized as a benchmark for evaluating causality discovery methods (Zhang et al., 2023; Lindner, Auret and Bauer, 2020). The diagram of the two-tank system is shown in Fig. 6.

When the input temperature  $T_{1,\text{in}}$  of the cold water experiences a step disturbance and thus drops rapidly, the temperature  $T_1$  in Tank 1 would follow a sharp decreasing trend. Then, the temperature controller TC1 increases the steam flow rate  $F_3$  to raise the temperature  $T_1$  in Tank 1. However, since the controller cannot completely counteract the disturbance, the temperature  $T_2$  in Tank 2 would decline

**Table 1**

Variables in the twotank system and their corresponding descriptions, high limits, and low limits.

| Variable   | Description   | High limit | Low limit |
|------------|---|------------|-----------|
| $T_{1,in}$ | Input temperature of cold water (°C)                | 25.1178    | 24.8842   |
| $F_3$      | Steam flow rate of the tank 1 (m <sup>3</sup> /min) | 0.5014     | 0.4974    |
| $F_4$      | Steam flow rate of the tank 2 (m <sup>3</sup> /min) | 0.0385     | 0.0382    |
| $T_1$      | Water temperature of the tank 1 (°C)                | 50.4253    | 49.4951   |
| $T_2$      | Water temperature of the tank 2 (°C)                | 50.4899    | 49.4100   |

**Table 2**

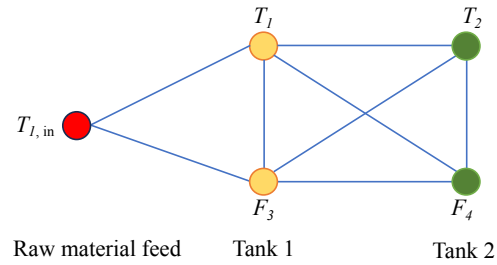
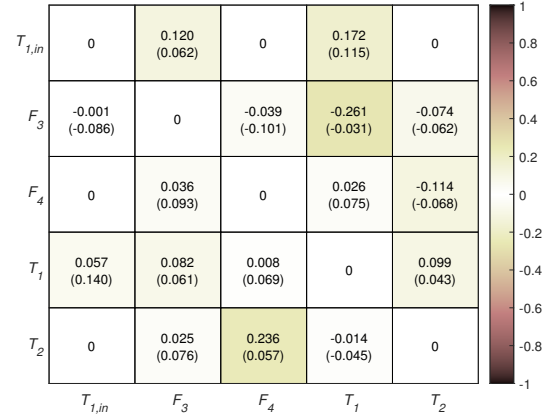
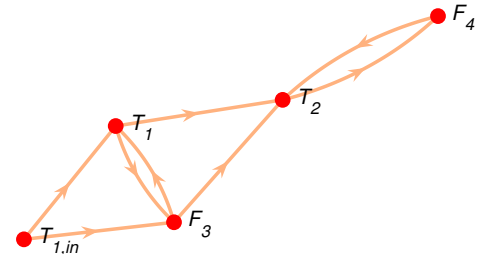
A partial example of the alarm event sequence generated by the two-tank system.

| Alarm tag  | Time stamp | Plant unit        |
|------------|------------|-------------------|
| $T_1$      | 13:13:05   | Tank 1            |
| $T_2$      | 13:15:05   | Tank 2            |
| $T_{1,in}$ | 13:17:21   | Raw material feed |
| $F_3$      | 13:17:22   | Tank 1            |
| $F_4$      | 13:18:37   | Tank 2            |
| $T_1$      | 13:20:57   | Tank 1            |
| $T_{1,in}$ | 13:21:21   | Raw material feed |
| $T_2$      | 13:21:29   | Tank 2            |
| $F_3$      | 13:22:35   | Tank 1            |

accordingly, which may trigger the temperature controller TC2 to increase the steam flow rate  $F_4$ , so as to compensate and elevate  $T_1$  in Tank 2. As a result, the rapid drop of  $T_{1,in}$  triggers a low limit alarm, which in turn excites a cascade of subsequent alarms, including low limit alarms of  $T_1$  and  $T_2$ , as well as high limit alarms of  $F_3$  and  $F_4$ . Further, the alarms triggered by the elevated steam flow rates  $F_3$  and  $F_4$  lead to a rise in the tanks' temperatures, which subsequently inhibits low limit alarms of  $T_1$  and  $T_2$ . In this alarm propagation process, five variables are involved; their descriptions and configured alarm limits are provided in Table 1.

A partial example of the alarm event sequence generated by the two-tank system is shown in Table 2. Based on the alarm event sequence, the NPP model is established using the method in Section 3.1. The process topology of the two-tank system is then derived from process flow diagrams and prior knowledge, as illustrated in Fig. 7. Subsequently, by incorporating the historical information of different alarms, the NCCI between alarms is calculated individually, with process topology as a constraint. The NCCI and threshold among the five alarms have been computed and are presented in Fig. 8. By comparing the calculated NCCIs with the thresholds, the causal relations between different alarms are determined. For example, from  $T_{1,in}$  to  $T_1$ ,  $NCCI_{T_{1,in} \rightarrow T_1} = 0.203$ , the threshold  $NCCI_{T_{1,in} \rightarrow T_1}^{\text{th}} = 0.108 < 0.203$ ; so there exist a causal relation from  $T_{1,in}$  to  $T_1$ . From  $F_4$  to  $F_3$ ,  $NCCI_{F_4 \rightarrow F_3} = 0.029$ , the threshold  $NCCI_{F_4 \rightarrow F_3}^{\text{th}} = 0.068 > 0.029$ ; so there no causal relation exists.

The causal graph depicting the relationships among the alarms is illustrated in Fig. 9, while the corresponding root

**Fig. 7:** Process topology of the two-tank system.**Fig. 8:** NCCIs and thresholds (in the brackets) of different alarms for two-tank system.**Fig. 9:** The causal graph by the proposed method.

cause ranking scores are presented in Fig. 10. It can be seen that  $T_{1,in}$  clearly stands out as the root alarm, triggering the other alarms and achieving the highest root cause ranking score. Fig. 9 shows that when  $T_{1,in}$  is abnormal, the temperature  $T_1$  and flow  $F_3$  of the first tank are also affected and become abnormal. As the process continues to run, abnormalities subsequently appear in the temperature  $T_2$  and flow  $F_4$  of the second tank. Moreover, the identified causal relations among the alarms depicted in Fig. 9 are consistent with the previous analysis.

#### 4.2. Case 2: Vinyl Acetate Monomer

The VAM plant model is a public dynamic model that simulates the VAM process (Luyben and Tyréus, 1998; Yang, Hu, Cao and Wu, 2020). It is comprised of eight

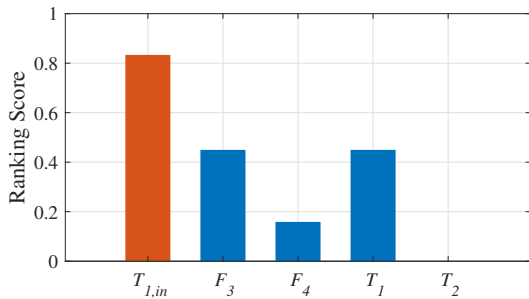


**Fig. 10:** Root cause ranking score for two-tank system.

major unit sections, including the material feed section, reactor, separator and compressor, absorber, buffer tank, CO<sub>2</sub> remover and purge line, distillation column, as well as decanter. Alarms were configured in the model to construct an alarm system and produce the A&E data (Yang et al., 2020). The alarm configuration covers critical process variables, including flow rates, temperatures, pressures, and composition measurements across different units, providing comprehensive monitoring of the process states.

#### 4.2.1. Analysis of the alarm propagation mechanism in VAM model

In the VAM model, the fault numbered “MAL 15” is a typical fault: Fail Absorber Circulation Pump. It is caused by the failure of the absorber’s circulation pump. When this fault occurs, the flow controller FC430 quickly drops to 0 and an alarm is generated. This is because FC430 is used to maintain the circulation flow rate of the absorber. After that, the fault will propagate along the material flow path, affecting the operation process of the entire absorber, and more and more alarms will appear one after another.

For example, due to the rapid decrease in the circulation flow rate, the absorption process in the absorber will also be abnormal, and the pressure difference between the bottom and the top of the absorber will change, and the alarm PDI401 will appear. In addition, after the absorption in the absorber is completed, the various gases output upward will also change their flow rate, causing the flow indicators FI402 and FI403 to alarm. And the various liquids output downward from the absorber will also change its flow rate, causing the flow indicator FI401 to alarm, and the level controller LC401 to alarm.

It can be seen that there is a relationship between these alarms triggered by the fault. Digging out the causal relations between these alarms and locating the root alarm can effectively guide the operator to handle and eliminate the alarm. The process diagram of the absorber and other related processes is shown in Fig. 11. The related variables are given in Table 3.

#### 4.2.2. Performance evaluation of the proposed method

To evaluate the effectiveness of the proposed alarm causality discovery method, experiments were conducted using the VAM model with the fault “MAL 15” configured

**Table 3**  
Variables and corresponding description in VAM model.

| Variable | Description  |
|----------|--|
| FC430    | Control circulation flow rate                          |
| FC460    | Control purge gas flow                                 |
| LC401    | Control bottom level of the absorber                   |
| TC410    | Control circulation flow temperature                   |
| TC420    | Control top feed flow temperature                      |
| FI401    | Flow of AcOH, H <sub>2</sub> O, and VAM from absorber  |
| FI402    | Flow of various gases                                  |
| FI403    | Flow of various gases after CO <sub>2</sub> separation |
| FI471    | Flow of various liquids from absorber and separator    |
| PDI401   | Pressure difference in absorber                        |
| QI400    | Quality of O <sub>2</sub>                              |
| QI410    | Quality of AcOH  |
| QI460    | Quality of C <sub>2</sub> H <sub>6</sub>               |

as the test scenario. The alarm event sequence data was collected over a one-week period under this fault condition.

Subsequently, the NCCI between alarms is calculated individually, with process topology as a constraint. The NCCI and corresponding thresholds among the 13 alarms have been computed and are presented in Fig. 12. By comparing the calculated NCIs with the thresholds, the causal relations between different alarms are determined. This causality discovery approach provides a clear delineation between causal and non-causal relationships, enabling precise identification of the root cause alarm.

The causal graph illustrating the relationships among the 13 alarms is shown in Fig. 13, with the corresponding root cause ranking scores presented in Fig. 14. These figures reveal that FC430 achieves the highest root cause ranking score, significantly surpassing all other alarms. The graph structure confirms FC430’s role as the primary root cause, characterized by minimal upstream influence and extensive causal pathways to multiple downstream alarms such as FI402, QI460, PD401, and others through complex interconnections. In comparison, other variables have considerably lower scores, reflecting their roles as intermediate or terminal nodes in the causal chain.

This identified root alarm is consistent with the physical understanding that a circulation pump failure first affects the flow controller. Further, the identified causal relations among these alarms are consistent with the prior analysis of the alarm propagation mechanism. The results reveal a structured pattern of alarm propagation that follows the physical flow paths within the absorber system. This demonstrates the effectiveness of the proposed method in uncovering causal relations and identifying root alarms.

In addition, to evaluate the impact of system topology on the proposed method, a comparative analysis without topology constraints is conducted. The causal graph and root cause ranking scores generated without considering system topology are shown in Figs. 15 and 16, respectively. Notably, Fig. 15 depicts a much denser graph compared to the graph in Fig. 13 that exploits system topology constraints.

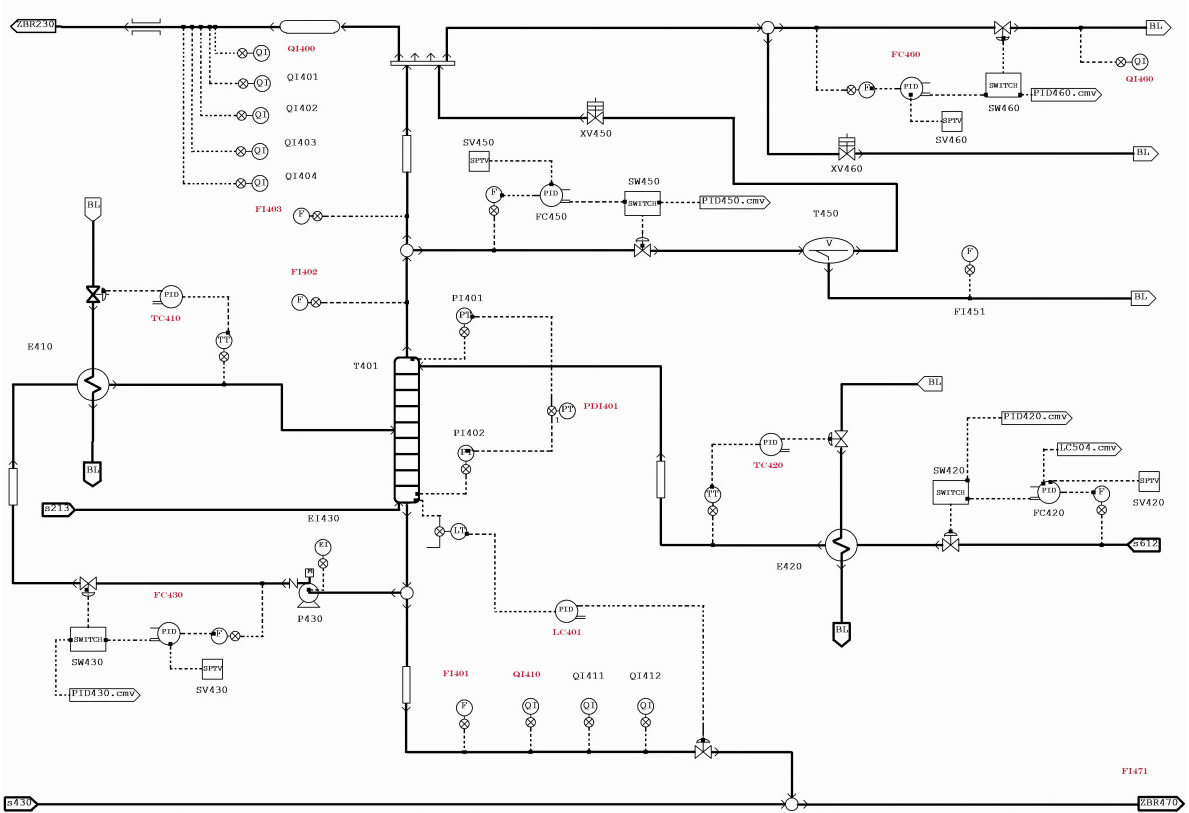


**Fig. 11:** The process diagram of the absorber and other related processes in VAM model.

|        |                  |                  |                    |                    |                  |                    |                    |                  |                    |                    |                    |                  |                    |
|--------|------------------|------------------|--------------------|--------------------|------------------|--------------------|--------------------|------------------|--------------------|--------------------|--------------------|------------------|--------------------|
| FC430  | 0                | 0                | -0.140<br>(-0.024) | -0.200<br>(-0.010) | 0                | 0                  | 0.286<br>(0.156)   | 0                | 0                  | 0.420<br>(0.216)   | 0                  | 0                | 0                  |
| FC460  | 0                | 0                | 0.064<br>(0.160)   | 0                  | 0                | 0                  | 0.034<br>(0.217)   | 0                | 0                  | 0.130<br>(0.084)   | 0                  | 0                | -0.018<br>(-0.076) |
| LC401  | 0.038<br>(0.093) | 0.120<br>(0.056) | 0                  | 0.028<br>(0.116)   | 0                | 0.004<br>(0.076)   | 0.018<br>(0.166)   | 0.072<br>(0.132) | 0                  | 0.372<br>(0.228)   | 0.172<br>(0.092)   | 0.058<br>(0.110) | -0.062<br>(-0.144) |
| TC410  | 0.036<br>(0.079) | 0                | -0.090<br>(-0.174) | 0                  | 0                | 0                  | 0.160<br>(0.112)   | 0                | 0                  | 0.030<br>(0.086)   | 0                  | 0                | 0                  |
| TC420  | 0                | 0                | 0                  | 0                  | 0                | 0                  | 0.094<br>(0.268)   | 0                | 0                  | 0                  | 0                  | 0                | 0                  |
| FI401  | 0                | 0                | 0.046<br>(0.116)   | 0                  | 0                | 0                  | 0                  | 0                | 0.038<br>(0.280)   | 0                  | 0                  | 0                | 0                  |
| FI402  | 0                | 0                | 0                  | 0                  | 0.010<br>(0.120) | 0                  | 0                  | 0.170<br>(0.091) | 0                  | -0.676<br>(-0.252) | 0.242<br>(0.112)   | 0                | 0.120<br>(0.032)   |
| FI403  | 0                | 0                | 0.020<br>(0.052)   | 0                  | 0                | 0                  | -0.002<br>(-0.296) | 0                | 0                  | 0.046<br>(0.204)   | -0.022<br>(-0.068) | 0                | 0                  |
| FI471  | 0                | 0                | 0                  | 0                  | 0                | -0.032<br>(-0.144) | 0                  | 0                | 0                  | 0                  | 0.328<br>(0.240)   | 0                | 0                  |
| PDI401 | 0                | 0                | 0                  | 0                  | 0.386<br>(0.089) | 0                  | 0.060<br>(0.156)   | 0                | 0                  | 0                  | 0.004<br>(0.074)   | 0.430<br>(0.180) | -0.172<br>(-0.043) |
| QI400  | 0                | 0                | -0.004<br>(-0.020) | 0                  | 0                | 0                  | -0.010<br>(-0.304) | 0.008<br>(0.136) | 0                  | 0.058<br>(0.132)   | 0                  | 0                | 0                  |
| QI410  | 0                | 0                | 0.028<br>(0.091)   | 0                  | 0                | 0.306<br>(0.168)   | 0                  | 0                | -0.520<br>(-0.108) | 0                  | 0                  | 0                | 0                  |
| QI460  | 0                | 0.004<br>(0.061) | 0.002<br>(0.069)   | 0                  | 0                | 0                  | 0.0584<br>(0.148)  | 0                | 0                  | -0.002<br>(-0.082) | 0                  | 0                | 0                  |

**Fig. 12:** NCCIs and thresholds (in the brackets) of different alarms for VAM model.

This increased density leads to spurious causal connections between physically disconnected systems, such as the incorrect causal link between alarms TC420 and FI471. Even though, if only observing the root cause variable, the result is consistent with considering system topology constraints, as demonstrated in Fig. 16, where FC430 retaining the

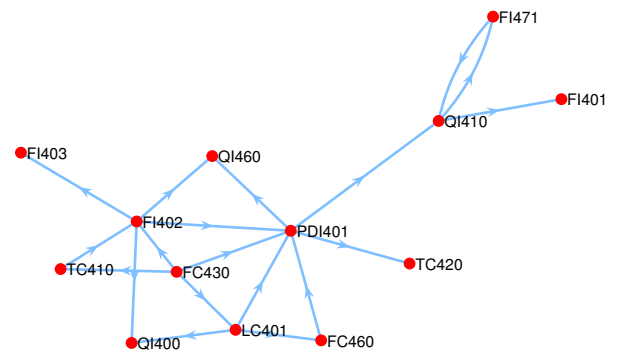


**Fig. 13:** The causal graph for the VAM model by the proposed method.

highest ranking score is identified as the root cause variable. In conclusion, while process topology is crucial for causal discovery to identify the correct alarm propagation path, its absence does not critically compromise root cause identification, highlighting both the importance of topology constraints for interpretable results and the robustness of the root cause analysis.

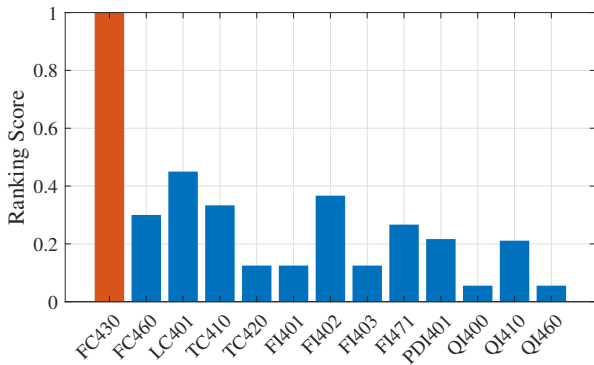


**Fig. 14:** Root cause ranking score for VAM model

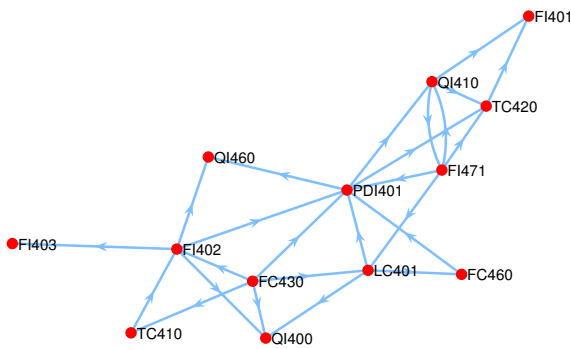


**Fig. 15:** The causal graph for the VAM model by the proposed method without system topology.

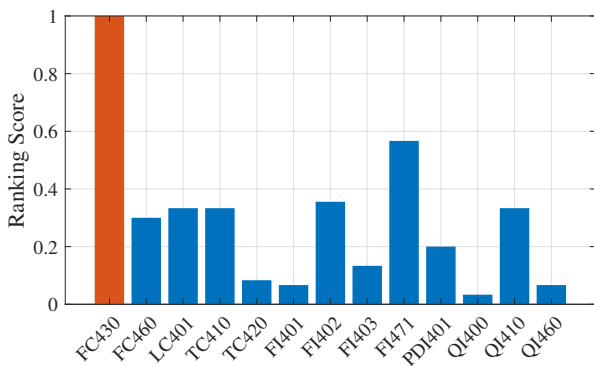


**Fig. 16:** Root cause ranking score from causal graph by the proposed method without system topology.

#### 4.2.3. Comparison

To demonstrate the advantages of the proposed method, three causality discovery methods were employed for comparison. These include two methods based on traditional point processes using A&E data: HP (Xu et al., 2016) and THP (Cai et al., 2024), as well as one method utilizing binary alarm series: TE (Hu et al., 2017), where the binary alarm series is converted from A&E data.

The HP method models the excitation between alarm events using fixed exponential kernels, which assumes uniform temporal influence patterns across all alarm pairs. THP extends the HP approach by incorporating system topology as a constraint but still relies on parametric kernels with limited expressiveness. The TE method measures information transfer between binary alarm signals rather than the more informative event data. The causal graphs generated by the HP, THP, and TE are shown in Fig. 17. These graphs reveal significant structural differences in the identified causal relationships. The TE method (Fig. 17(c)) produces causal graphs with many spurious connections, and some key alarm variables are not taken into account. The HP method (Fig. 17(a)) shows better discrimination but still includes several incorrect causal links. The THP method (Fig. 17(b)) demonstrates improved performance through topology integration, though certain causal relationships remain misidentified.

By comparing the causal graphs of different methods, it is found that the causal graph generated by the proposed method closely aligns with the previously established alarm propagation path during the fault “MAL 15”. Further, the causal graphs of different methods were compared to the actual causal graph, and the accuracy of each method was calculated using the estimated causal matrix in relation to the actual causal matrix. Additionally, the number of incorrectly identified causal edges was counted, and the proportion of these errors relative to the total number of actual causal edges was calculated; this can be referred to as the misidentification rate. A lower misidentification rate indicates a more reliable method. This is crucial in practical industrial processes, as incorrect identification of causal relationships can significantly impact operators’ decisions, leading to inappropriate responses, which are often unacceptable in industrial processes.

The accuracy and misidentification rates of the different methods are presented in Table 4. It shows that the proposed method not only maintains a high level of accuracy (0.917 compared to 0.814 from THP) but also achieves the lowest misidentification rate (0.071 compared to 0.286 from THP). The substantial improvement in misidentification rate (75.2% reduction compared to THP) is particularly significant, as it directly translates to increased reliability in root cause identification. This demonstrates the effectiveness and reliability of the proposed causality discovery method in uncovering the causal relations between alarm events. In addition, the computation time of different methods is presented in Table 4. It can be seen that the proposed method is the fastest, finishing in roughly one-fourth the time required by HP and THP, while TE is the slowest by a wide margin. All simulations were conducted on a 64-bit Windows PC with Intel Core i5-1135G7 CPU @ 2.40 GHz and 16.0 GB RAM.

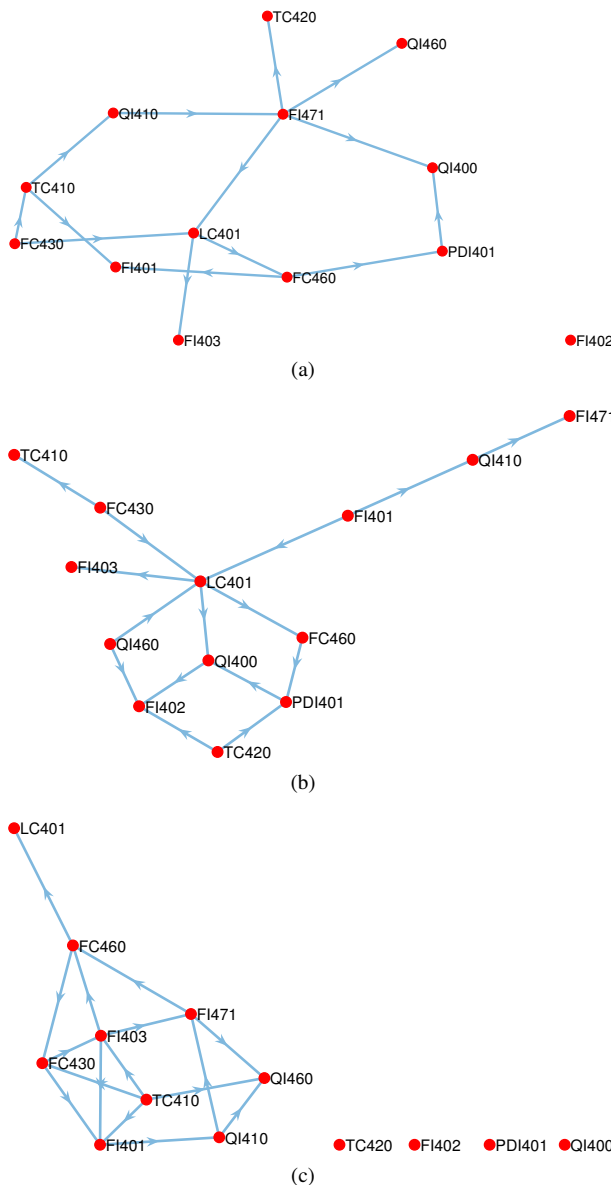
## 5. Conclusions

This study proposes an alarm causality discovery method based on the neural point process and Granger causality.

**Table 4**

Accuracy, misidentification rate, and computation time of different methods.

|                        | HP (Xu et al., 2016) | THP (Cai et al., 2024) | TE (Hu et al., 2017) | AlarmCNPP    |
|------------------------|----------------------|------------------------|----------------------|--------------|
| Accuracy               | 0.795                | 0.814                  | 0.731                | <b>0.917</b> |
| Misidentification rate | 0.321                | 0.286                  | 0.536                | <b>0.071</b> |
| Computation time       | 46.9 s               | 41.7 s                 | 492.8 s              | 11.6 s       |

**Fig. 17:** The causal graphs for the VAM model by different methods. (a) HP. (b) THP. (c) TE.

In contrast to methods that rely on process data, this paper directly utilizes A&E data for causality discovery. First, a NPP modeling method based on alarm encoding and CTL-STM is proposed for A&E data to compute the conditional intensity. A new causality measurement, referred to as CCI, is then designed, which is based on conditional intensity and normalized to facilitate the analysis of causal relations

between alarms. In addition, the system topology is extracted as a constraint to eliminate spurious causal relations. By analyzing the causal relations and identifying the root cause alarms, this approach provides decision support for operators managing alarms. The effectiveness of the proposed method is demonstrated through validation on two public industrial models.

## CRediT authorship contribution statement

**Xiangxiang Zhang:** Writing - Original draft, Methodology, Investigation, Data curation. **Wenkai Hu:** Writing - review & editing, Supervision, Project administration, Funding acquisition, Conceptualization. **R. Bhushan Gopaluni:** Writing - review & editing, Validation, Formal analysis.

## Declaration of competing interest

The authors declare that they have no known competing financial interests or personal relationships that could have appeared to influence the work reported in this paper.

## Acknowledgments

This work was supported by the National Natural Science Foundation of China under Grant No. 62373335 and the Key Program of Hubei Provincial Technical Innovation Project under Grant No. 2023BAB080.

## References

- de Abreu, R.S., Nunes, Y.T., Guedes, L.A., Silva, I., 2021. A method for detecting causal relationships between industrial alarm variables using transfer entropy and k2 algorithm. *Journal of Process Control* 106, 142–154.
- Alinezhad, H.S., Roohi, M.H., Chen, T., 2022. A review of alarm root cause analysis in process industries: Common methods, recent research status and challenges. *Chemical Engineering Research and Design* 188, 846–860.
- Cai, R., Wu, S., Qiao, J., Hao, Z., Zhang, K., Zhang, X., 2024. THPs: Topological hawkes processes for learning causal structure on event sequences. *IEEE Transactions on Neural Networks and Learning Systems* 35, 479–493.
- Duan, S., Zhao, C., Wu, M., 2023. Multiscale partial symbolic transfer entropy for time-delay root cause diagnosis in nonstationary industrial processes. *IEEE Transactions on Industrial Electronics* 70, 2015–2025.
- Hu, W., Wang, J., Chen, T., Shah, S.L., 2017. Cause-effect analysis of industrial alarm variables using transfer entropies. *Control Engineering Practice* 64, 205–214.
- Hu, W., Yang, G., Li, Y., Cao, W., Wu, M., 2024. Root cause identification of industrial alarm floods using word embedding and few-shot learning. *IEEE Transactions on Industrial Informatics* 20, 1465–1475.

- Jiang, H., Patwardhan, R., Shah, S.L., 2009. Root cause diagnosis of plant-wide oscillations using the concept of adjacency matrix. *Journal of Process Control* 19, 1347–1354.
- Kathari, S., Tangirala, A.K., 2022. A novel framework for causality analysis of deterministic dynamical processes. *Industrial & Engineering Chemistry Research* 61, 18426–18444.
- Kumari, P., Bhadriraju, B., Wang, Q., Kwon, J.S.I., 2022. A modified bayesian network to handle cyclic loops in root cause diagnosis of process faults in the chemical process industry. *Journal of Process Control* 110, 84–98.
- Landman, R., Jämsä-Jounela, S.L., 2019. Fault propagation analysis by implementing nearest neighbors method using process connectivity. *IEEE Transactions on Control Systems Technology* 27, 2058–2067.
- Lin, H., Tan, C., Wu, L., Liu, Z., Gao, Z., Li, S.Z., 2025. An extensive survey with empirical studies on deep temporal point process. *IEEE Transactions on Knowledge and Data Engineering* 37, 1599–1619.
- Lindner, B., Auret, L., Bauer, M., 2020. A systematic workflow for oscillation diagnosis using transfer entropy. *IEEE Transactions on Control Systems Technology* 28, 908–919.
- Lindner, B., Auret, L., Bauer, M., Groenewald, J.W., 2019. Comparative analysis of granger causality and transfer entropy to present a decision flow for the application of oscillation diagnosis. *Journal of Process Control* 79, 72–84.
- Luo, Y., Gopaluni, B., Cao, L., Wang, Y., Cheng, J., 2023. Adaptive online optimization of alarm thresholds using multilayer bayesian networks and active transfer entropy. *Control Engineering Practice* 137, 105534.
- Luo, Y., Gopaluni, B., Xu, Y., Cao, L., Zhu, Q.X., 2020. A novel approach to alarm causality analysis using active dynamic transfer entropy. *Industrial & Engineering Chemistry Research* 59, 8661–8673.
- Luyben, M.L., Tyréus, B.D., 1998. An industrial design/control study for the Vinyl Acetate Monomer process. *Computers & Chemical Engineering* 22, 867–877.
- Mei, H., Eisner, J.M., 2017. The neural hawkes process: A neurally self-modulating multivariate point process. *Advances in Neural Information Processing Systems* 30.
- Nielsen, E.K., Gofuku, A., Zhang, X., Ravn, O., Lind, M., 2020. Causality validation of multilevel flow modelling. *Computers & Chemical Engineering* 140, 106944.
- Rahaman, M.H., Alinezhad, H.S., Chen, T., 2024. Identification of most critical alarms for alarm flood reduction. *IFAC-PapersOnLine* 58, 835–840.
- Song, P., Zhao, C., Huang, B., Wu, M., 2022. Sparse and time-varying predictive relation extraction for root cause quantification of nonstationary process faults. *IEEE Transactions on Instrumentation and Measurement* 71, 1–13.
- Tank, A., Covert, I., Foti, N., Shojaie, A., Fox, E.B., 2022. Neural granger causality. *IEEE Transactions on Pattern Analysis and Machine Intelligence* 44, 4267–4279.
- Wang, J., Hu, W., Chen, T., 2024. *Intelligent Industrial Alarm Systems*. Springer.
- Xiao, S., Yan, J., Farajtabar, M., Song, L., Yang, X., Zha, H., 2019. Learning time series associated event sequences with recurrent point process networks. *IEEE Transactions on Neural Networks and Learning Systems* 30, 3124–3136.
- Xu, H., Farajtabar, M., Zha, H., 2016. Learning granger causality for hawkes processes, in: International Conference on Machine Learning, PMLR. pp. 1717–1726.
- Yang, F., Duan, P., Shah, S.L., Chen, T., 2014. *Capturing Connectivity and Causality in Complex Industrial Processes*. Springer Science & Business Media.
- Yang, F., Xiao, D., Shah, S.L., 2013. Signed directed graph-based hierarchical modelling and fault propagation analysis for large-scale systems. *IET Control Theory & Applications* 7, 537–550.
- Yang, G., Hu, W., Cao, W., Wu, M., 2020. Simulating industrial alarm systems by extending the public model of a Vinyl Acetate Monomer process, in: 2020 39th Chinese Control Conference (CCC), pp. 6093–6098.
- Yang, X., Lan, T., Qiu, H., Zhang, C., 2025. Nonlinear causal discovery via dynamic latent variables. *IEEE Transactions on Automation Science and Engineering* 22, 10381–10391.
- Yu, W., Yang, F., 2015. Detection of causality between process variables based on industrial alarm data using transfer entropy. *Entropy* 17, 5868–5887.
- Zhang, X., Hu, W., Al-Dabbagh, A.W., Wang, J., 2024. Improved similarity analysis of industrial alarm flood sequences by considering alarm correlations. *Journal of Process Control* 142, 103295.
- Zhang, X., Hu, W., Yang, F., Cao, W., Wu, M., 2023. A new transfer entropy approach based on information granulation and clustering for root cause analysis. *Control Engineering Practice* 140, 105669.
- Zhao, L., Song, P., Zhao, C., 2025. Causal similarity learning with multi-level predictive relation aggregation for grouped root cause diagnosis of industrial faults. *Control Engineering Practice* 154, 106140.